Cation permeability and pore dynamics in TRPV1 ion channels.

Miriam García-Ávila[1], Javier Tello-Marmolejo[1,2], Tamara Rosenbaum[3] and León D. Islas[1*]

From:

[1]Department of Physiology, School of Medicine, UNAM, Mexico City, 04510, Mexico.

[2]Current affiliation: Department of Physics, University of Gothenburg, 405 30 Gothenburg, Sweden.

[3]Department of Cognitive Neuroscience, Instituto de Fisiología Celular, UNAM, Mexico City, 04510, Mexico.

*Correspondence to:

León D. Islas

Department of Physiology

School of Medicine

Universidad Nacional Autónoma de México (UNAM)

Circuito Escolar S/N, Ciudad Universitaria

Ciudad de México, 04510, México

leon.islas@gmail.com

ORCIDs

Javier Tello-Marmolejo: https://orcid.org/0000-0002-3665-793

L.D. Islas: https://orcid.org/0000-0002-7461-5214

Miriam García-Ávila: https://orcid.org/0000-0002-5326-7302

Tamara Rosenbaum: https://orcid.org/0000-0002-4791-3195

Abstract

The Transient Receptor Vanilloid (TRPV) 1 is a non-selective ion channel which is activated by several chemical ligands and heat. We have previously shown that activation of TRPV1 by different ligands result in single-channel openings with different conductance, suggesting that the selectivity filter is highly dynamic. TRPV1 is weakly voltage-dependent, here we sought to explore whether the permeation of different monovalent ions could influence the voltage-dependence of this ion channel. By using single-channel recordings, we show that TRPV1 channels undergo rapid transitions to closed states that are directly connected to the open state, which may result from structural fluctuations of their selectivity filters. Moreover, we demonstrate that the rates of these transitions are strongly influenced by the permeant ion, suggesting that ion permeation regulates the voltage dependence of these channels.

Introduction

Transient receptor potential vanilloid (TRPV) are members of a superfamily of voltage-gated-like ion channels (Yu and Catterall, 2004). The first member of the TRPV family to be identified was TRPV1, which is a non-selective cationic channel involved in thermal sensation and which participates in the physiology of pain and inflammation (Rosenbaum et al., 2022). TRPV1 channels assemble as homotetramers, and each subunit contains large intracellular N-and C-terminal domains of complex architecture (Liao et al., 2013), and a transmembrane domain formed by six alpha helical membrane-spanning segments. Within this transmembrane domain, the transmembrane helices S1 to S4 form a helix bundle constituting a voltage sensor-like domain (VSLD), that does not seem to function as the voltage-sensor domains (VSD) present in canonical voltage-activated channels (Palovcak et al., 2015a), but which contains multiple binding sites for activating and regulatory molecules (Cao, 2020).

55 The pore, which contains a selectivity filter and an activation gate, is formed by the S5
56 segment, a pore loop and a helix motif and the S6 segment (Liao et al., 2013).

57 TRPV1 can be activated by varied stimuli such as capsaicin, external pH < 5.4, heat,
58 various ligands and voltage (Caterina and Julius, 2001; Jordt et al., 2000; Matta and
59 Ahern, 2007; Grandl et al., 2010; Rosenbaum et al., 2022). Interactions with these
60 stimuli lead to widening of the S6 activation gate, culminating in channel opening and
61 ion permeation (Salazar et al., 2009). Importantly, these activating factors are
62 allosterically coupled to the channel gate and also between them (Jara-Oseguera and
63 Swartz, 2015).

64 Several structures of TRPV1 and related channels (TRPV1-4) have been solved by X-
65 ray crystallography and cryoEM methods (Liao et al., 2013; Zubcevic et al., 2018;
66 Shimada et al., 2020; Deng et al., 2018). These structures show that in the presence of
67 activators, the selectivity filter (SF) can adopt varying conformations, suggesting that
68 in these channels the SF is a highly dynamic structure (Zubcevic et al., 2018).
69 Functional experiments have shown that, while not an activation gate, the SF shows
70 dynamic accessibility changes (Jara-Oseguera et al., 2019). It has also been suggested
71 that voltage-induced conformational changes in this structure underlie the very small
72 voltage dependence of activation (Yang et al., 2020).

73 The dynamic character of the selectivity filter of TRPV1 has not been studied
74 functionally, although several lines of evidence point towards this characteristic. For
75 example, different agonists of TRPV1 can open the channel to distinct single-channel
76 conductance levels (Canul-Sánchez et al., 2018; Geron et al., 2018). We decided to
77 characterize the effect of the permeant ions on gating of TRPV1, with emphasis on the
78 voltage-dependence of activation. We observed very rapid transitions to closed states
79 that are directly connected to the open state and that might represent structural
80 fluctuations of the SF. The rates of these transitions are strongly influenced by the
81 permeant ion, in a manner that is consistent with ion transport being involved in the
82 voltage dependence of these channels.

83

84 **Methods**

85 *Cell culture and transfection.*

86 We used the HEK293 cell line from American Type Culture Collection (ATCC; RRID:
87 CVCL_0045) for heterologous expression of TRPV1. Cells were grown in Dulbecco´s
88 Modified Eagle Medium (DMEM, Invitrogen) with the addition of 10% fetal bovine
89 serum (Invitrogen) and 1% of penicillin-streptomycin (Invitrogen) (referred to as
90 supplemented DMEM). Cultures were incubated at 37°C, in a 5 % CO_2 atmosphere.
91 Every 3 or 4 days the cells were washed with PBS, followed by treatment with 1 ml of
92 0.05% trypsin-EDTA (Invitrogen) for 2 min, then 1 ml of supplemented DMEM was
93 added. Subsequently, the cells were mechanically dislodged and 80 µl of the cell
94 suspension were reseeded in 30 mm culture dishes containing 5 x 5 mm glass
95 coverslips at the bottom and 2 ml of supplemented DMEM. After 1-2 days in culture,
96 cells were cotransfected with pcDNA3.1 plasmid with WT rat TRPV1 (rTRPV1) and
97 pEGFP-N1 plasmid containing the eGFP fluorescent protein using the jetPEI
98 transfection reagent (Polyplus), according to manufacturer's instructions. Single-
99 channel recordings were done one day after transfection, while macroscopic
100 recordings were performed two or more days after transfection.

101 *Electrophysiological recordings.*

102 The experiments were carried out in the inside-out configuration of the patch-clamp
103 recording technique (Hamill et al., 1981). Recordings were performed using a pipette
104 (extracellular) solution consisting of 130 mM NaCl, 10 mM HEPES and 5 mM EGTA, pH
105 7.4, and bath (intracellular) solutions in the pipette with either 130 mM NaCl, KCl,
106 RbCl, LiCl, NH_4Cl or CsCl (depending on the experiment, as indicated in the figure
107 legends), 10 mM HEPES, and 5 mM EGTA, pH 7.4.

108 Currents were recorded with an EPC-10 patch-clamp amplifier (RRID:SCR_018399,
109 HEKA Elektronik) controlled by PatchMaster software (RRID:SCR_000034, HEKA
110 Elektronik). Borosilicate capillaries (Sutter instruments) were used to fabricate patch-

111 pipettes, which had a resistance after fire polishing of 4-6 MΩ for macroscopic
112 currents and 8-10 MΩ for single-channel recordings.

113 Macroscopic currents were filtered at 1 kHz (low-pass Bessel), sampled at 40 kHz and
114 single-channel currents filtered at 5 kHz, sampled at 50 kHz.

115 *Analysis of macroscopic current recordings.*

116 The macroscopic conductance in each permeant ion condition was determined from
117 the current *I,* applying Ohm's law according to:

$$G = \frac{I}{V - V_{rev}}$$

118 where V is the test voltage and V_{rev} is the reversal potential. The conductance was
119 normalized to the maximum G_{max} and plotted as a function of voltage and was fit to a
120 Boltzmann function:

121 $$G/Gmax = \frac{1}{1+e^{-z(V-V_{1/2})/(K_B T)}} \qquad \text{Eq. 1}$$

122 where z is the apparent valence of gating in e_o, $V_{1/2}$ is the potential where G/G_{max}=0.5,
123 K_B is Boltzmann's constant and T the temperature in Kelvin.

124 *Analysis of single-channel recordings.*

125 Single-channel recordings were analyzed to determine the open probability, P_o.
126 Openings were detected employing the 50% threshold crossing method (Colquhoun
127 and Sigworth, 1995a). Single-channel traces were interpolated with a cubic spline
128 function before event detection. Open dwell time (d_o) and amplitude (a_o) of open
129 events and dwell times of closed events (d_c) were compiled and used to determine P_o
130 as:

131 $$P_o = \frac{d_o}{d_o + d_c} \qquad \text{Eq. 2}$$

132 The dwell times were also used to construct amplitude vs. open dwell time
133 relationships.

134 *Analysis of fast single-channel current fluctuations.*

Fast current fluctuations are apparent in single-channel records both as increases in the open-channel noise and as incomplete closing transitions. Since the half-amplitude crossing method is not appropriate to study these extremely fast events, we chose to analyze these fast kinetics by studying the all-points amplitude histograms compiled from bursts of channel activity, employing an extension of the Beta-distribution analysis developed by (Schroeder, 2015), which is applicable to systems with more than two states. This analysis relies on fitting of the all-points amplitude histograms to theoretical distributions derived from time series of simulated channel activity from specific kinetic models. These fits yield forward and backward rate constants that were analyzed over varying conditions of permanent ion and voltages.

Model fitting.

A simulated time series of channel openings and closings from specific Markov models of gating was first generated employing a Monte Carlo method. For exponentially distributed dwell times, any particular, random duration of value d_i, in any closed or open state, i, is calculated from rate constants as in:

$$d_i = -\frac{1}{\sum_{i=1}^{j\neq i} k_{ij}} lnR_n \qquad \text{Eq. 3}$$

Here, k_{ij} are the rate constants leaving state i into state j and R_n is a uniformly distributed random number from 0 to 1. Transition probabilities between sates i and j, p_{ij} were calculated according to:

$$p_{ij} = k_{ij} / \sum_{i=1}^{j\neq i} k_{ij}$$

Once a time series is simulated, it is filtered by convolution with the impulse response of a Gaussian filter given by (Colquhoun and Sigworth, 1995b):

$$H(t) = \frac{1}{2\pi^{1/2}\sigma_g} exp\left(\frac{-t^2}{2\sigma_g^2}\right) \qquad \text{Eq. 4}$$

σ_g is related to the filter corner frequency f_c by:

$$\sigma_g = \frac{\sqrt{(ln2)}}{2\pi f_c}.$$

Simulated and filtered data are converted to an all-points amplitude histogram which is then fitted to the experimental histogram using a least-squares procedure and the fit parameters used to simulate a new time series until the fit error is minimized.

Experimental amplitude histograms were fitted to simulated histograms resulting from several models considering one open estate and two or more closed states with appropriate voltage dependent rate constants.

Fit to rate constants.

The voltage-dependence of each transition was calculated by plotting the rate constants as a function of voltage and by fitting the data to the following function:

$$k = k(0) \cdot e^{\left(\frac{z\,V}{K_B T}\right)} \qquad \text{Eq. 5}$$

Here, $k(0)$ is the rate constant at 0 mV, z is the apparent charge associated with the transition, K_B is the Boltzmann constant, T is the temperature (298°K) and V is the voltage applied.

Fast transitions showed saturation at high voltages and were thus fitted using a subtraction of two exponential functions:

$$k = k(0)_1 \cdot e^{\left(\frac{z_1 V}{K_B T}\right)} - k(0)_2 \cdot e^{\left(\frac{z_2 V}{K_B T}\right)} \text{ Eq. 6}$$

Data were analyzed with Patchmaster (HEKA) and custom-written programs in Igor Pro 8 (RRID: SCR_000325, Wave-Metrics) and Python 3 using Jupyter Notebooks (RRID:SCR_008394).

Statistical tests.

Statistical comparisons were made by using one-way ANOVA with significance determined from Tukey´s post hoc test. *$p < 0.05$ indicates statistical significance.

Results

185 In these experiments, we will focus on outward currents carried by varying permeant
186 ions, in the nominal absence of divalent ions and presence of a constant extracellular
187 concentration of NaCl. These conditions were chosen since it has been shown that Ca^{2+}
188 can permeate, block and produce Ca^{2+}-calmodulin mediated desensitization of TRPV1
189 (Rosenbaum et al., 2004; Numazaki et al., 2003) and that extracellular Na^+ ions are
190 required for normal gating in TRPV1 (Jara-Oseguera et al., 2016).

191 *Permeation and voltage dependence of TRPV1.*

192 Macroscopic currents through TRPV1 were activated by a saturating concentration of
193 capsaicin of 10 μM and recorded in asymmetric ion concentrations, with Na^+ always
194 present at 130 mM in the extracellular face of the channel. Outward currents were
195 carried by the test ion and were always preceded by recording of current in
196 symmetric Na^+ in the same patch, allowing the results to be compared over multiple
197 patches, taking as reference the condition in which the channel permeates Na^+ in both
198 directions, for example, red traces for only Na^+ vs. blue traces for Na^+/Li^+(Figure 1A).

199 As can be seen from I-V curves normalized to the current in Na^+ at 130 mV, TRPV1
200 permeates monovalent ions (Figure 1B) (Caterina et al., 1997a). Outward macroscopic
201 currents are larger when the permeant ion has a larger ionic radius like Cs^+ (1.6 $\dot{A}$).
202 However, the reversal potential was not statistically different from zero for each ion
203 tested (Figure 1B), showing that the channel does not select between monovalent
204 ions. Conductance (G) vs. voltage (V) relationships, again, normalized to G_{Na}, show that
205 the magnitude of the maximal conductance at positive voltages (G_{max}) depends on the
206 permeant ion. These G-V curves were fitted to Eq. 1, to estimate apparent charge, z
207 and voltage of half activation $V_{1/2}$. Besides the effect on G_{max}, the values of z and $V_{1/2}$,
208 are different for each of the permeant ions studied; specifically, there is a significant
209 difference in the ΔΔG with Li^+ (Compared to Na^+, Figure 1, D and E), which is brought
210 about by a significant increase in z (increased steepness of the G-V curve) and a
211 negative shift of the $V_{1/2}$.
212 To understand why the macroscopic conductance is affected by the permeant ion, we
213 performed single-channel recordings in identical ionic conditions. Our single-channel

214 recordings in the inside-out configuration show a clear increase in the microscopic
215 conductance when larger ions permeate. Based on the size of the single-channel
216 conductance, relative to the single-channel conductance of Na^+ current in the same
217 patch, we can estimate a permeability sequence as: $Li^+ < Na^+ < K^+ < Rb^+ < NH_4^+ < Cs^+$
218 (Figure 2A). The estimation of permeability was carried out since the reversal
219 potential was very close to zero for all ions (Figure 2 B) and thus a selectivity
220 sequence cannot be obtained.

221 Although the single-channel conductance explains in part the larger macroscopic
222 conductance when the permeant ion has a larger atomic radius, i.e., larger single-
223 channel conductance corresponds to larger macroscopic conductance, the microscopic
224 current-amplitudes observed by measuring single-channels (Figure 2B and C) do not
225 fully correspond to what is observed in macroscopic currents (Figure 1C). Specifically,
226 the single-channel conductance with Rb^+ is greater than in K^+, Na^+ and Li^+, unlike the
227 macroscopic results, where the conductance with Rb^+ is almost the lowest, only
228 comparable with the conductance with Li^+.

229 This difference suggests that when Rb^+ is the permeant ion at positive voltages, the
230 channel might gate differently. To test this possibility, we measured the single-
231 channel open probability according to Eq. 2, with different permeant ions. Figure 3A
232 shows that in the presence of Rb^+, the channel opens in short bursts, unlike thezzz
233 openings in Na^+, which happen in long-lived bursts. Concurrently, the open probability
234 is significantly smaller with Rb^+, while it is close to maximum in all other ions tested
235 (Figure 3B). This result reconciles the observed effects of ions on microscopic and
236 macroscopic conductance and reveals that the permeant ion modulates gating of
237 TRPV1. In particular, Rb^+ makes TRPV1 gate with lower open probability.

238 TRPV1 single-channel currents show a complex temporal structure; the open state is
239 rather unstable, showing many rapid closures or flickers and an increased open
240 channel noise. We observed that current flicker seems to get more noticeable with
241 increasing ion size and voltage (Figure 2A), suggesting that this flickery gating is a
242 phenomenon that arises from the interaction of the permeant ion with the pore of the
243 channel.

244 Increased open channel noise can occur when channels undergo very rapid
245 transitions to closed states adjacent to the open state (Rauh et al., 2018). These
246 dynamics can be seen as excess noise in the power spectrum of the open channel
247 current or as a non-Gaussian distribution of the all-points current amplitude
248 histogram (Heinemann and Sigworth, 1991). It has been shown that for a two-state
249 process, such as a unimolecular fast open channel block, the kinetics of the process
250 can be characterized from all-points current amplitude histograms by means of fitting
251 a beta distribution, which gives the amplitude of open events derived from a filtered
252 two-state stochastic process (Fitzhugh, 1983; Yellen, 1984).

253 When the fast process involves more than two states, there is no exact analytic
254 solution; however, it has been shown that the amplitude histograms can still be
255 compared with theoretical distributions derived from a simulation of a theoretical,
256 infinite bandwidth process filtered with the same filter and frequency of experimental
257 data. In this way, different explicit Markov models can be used to extract rate
258 constants from extended beta distributions (Rauh et al., 2017; Schroeder, 2015).

259 Bursts of openings of TRPV1 contain both excess noise and apparently incomplete
260 closures (Figure 4A), these two phenomena give rise to "tails" of excess low amplitude
261 events in the all-points current amplitude histograms. Interestingly these tails become
262 more prominent when channels conduct larger ions.

263 Figure 4B compares histograms for all ions tested at 90 mV. It can be observed that
264 the smaller ions (Li^+ and Na^+) produce amplitude histograms that are roughly
265 Gaussian, while for the larger ions, the histograms deviate from Gaussian and are
266 asymmetric, with increased counts at the left arm of the histogram formed by
267 amplitude values nearer to the closed amplitude. This is made more evident in Figure
268 4C, which scales the histograms to the maximum open amplitude for all ions. To
269 extract rate constants for the fast processes that give rise to these tails, we employed
270 extended beta distributions derived from the following Scheme I:

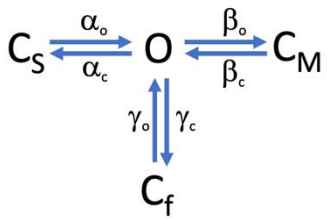

This scheme postulates the existence of three closed transitions adjacent to an open state, each transition representing a slow, intermediate and fast equilibrium given by alpha, beta and gamma rate constants, respectively. Although it is known that TRPV1 channels have many open and closed states, this simplified scheme can be applied to the study of bursts of openings at sub saturating capsaicin concentrations, since the effect of capsaicin is mainly to reduce the interburst interval (Hui et al., 2003).

This scheme generates gating behavior that is very similar to the experimentally observed busts (Figure 4D) and the derived all-points histograms provide a good fit to the experimental histograms (Figure 4E). We also tested two simpler schemes with one open and two closed states and show that these cannot provide an adequate fit to the data (Supplementary figure 1; green and blue traces, respectively).

The voltage dependence of the forward and backward rate constants obtained with the extended beta distribution method for all ionic conditions is shown in Figure 5. The slow opening transition (α_o) is determined mainly by longer lived closed states and shows a slight voltage dependence in all ions, except ammonium. Inversely, the closing transition (α_c) shows a higher voltage dependence. Intermediate opening and closing transitions (β_o and β_c) have less voltage dependence while the fast transitions (γ_o and γ_c) are again more voltage dependent. While the voltage-dependence of slow and intermediate rate constants can be fit to a single exponential function (Eq. 5), the fast-opening transitions show saturation at high positive voltages and can only be fitted with the subtraction of two exponential functions (Eq. 6), (see Table I for all fitted parameters). A very interesting finding derived from these measurements is that all rate constants are modulated by the permeant ion. In general, rate constants,

295 when compared at 0 mV, are faster with the larger ions such as Cs^+ and slower with
296 smaller ions, although this is not a rule.

297 The interplay between voltage and the effect of the permeant cation can be quantified
298 by the total charge associated with each of the three transitions, $Z_i = (z_i^o + z_i^c)$, where
299 i = α, β, γ and o, c represent the opening or closing rate constant, respectively. This is
300 plotted in Figure 5B for all ions. It is readily apparent that the smaller ions Li^+ and Na^+
301 are associated with a larger Z than say, Cs^+ or Rb^+. The finding that these transitions,
302 which occur near the open state, are voltage dependent with a relatively high
303 associated valence that depends on the size of the ion suggest that the observed
304 voltage-dependence of the macroscopic conductance might arise in part from the
305 movement of ions in the pore's electric field. This is consistent with our previous
306 observation that the macroscopic voltage dependence at a saturating capsaicin
307 concentration is modulated by the permeant ion (Figure 1D). To compare the
308 observed voltage dependence of rate constants with the macroscopic conductance, we
309 measured conductance at the same concentration of capsaicin at which rate constants
310 were estimated (100 nM) and compared it to the prediction of Scheme I, using the
311 measured rates and charges.

312 The open probability predicted by Scheme I is given by:

313 $$Po = \frac{K_\alpha}{1+K_\alpha+K_\alpha K_\beta+K_\alpha K_\gamma} \qquad \text{Eq. 7}$$

314 With equilibrium constants K_i given by:

315 $$K_i = \frac{i_o(0)e^{\frac{q_{i_o}V}{KT}}}{i_c(0)e^{\frac{q_{i_c}V}{KT}}} \qquad \text{Eq. 8}$$

316 Figures 6A depicts macroscopic currents measured at saturating (10 μM) and
317 subsaturating (100 nM) capsaicin. Figure 6C and D show G-V curves at 100 nM
318 capsaicin for all ions and the prediction of Scheme I (Eq. 7) using values derived from
319 measurements in Figure 5 (Table I). The model shows good agreement with the data
320 and shows that the estimated apparent charge associated with channel activation is
321 modulated by the permeant ion (Figure 6E).

322 **Discussion**

323 TRPV1 is generally characterized as a cation permeable, non-selective channel with
324 slightly higher permeability to Ca^{2+} ions (Caterina et al., 1997b). Surprisingly, little is
325 known of the permeation mechanisms for cations in TRPV1. A study by (Samways and
326 Egan, 2011) showed single-channel recordings at a negative voltage that suggested
327 non-selective permeability of cations (also based in single-channel conductance) in
328 the order: Na^+ > Cs^+ > Li^+ > K^+. In this study, we have employed single-channel
329 recordings under bi-ionic conditions and measured a permeability sequence based on
330 the conductance at positive voltages, where the single-channel conductance is higher
331 and easier to measure. We observed a sequence Cs^+ > Rb^+ > K^+ > Na^+ > Li^+.
332 Interestingly, this is consistent with an Eisenman sequence of type I (Eisenman,
333 1962), which is produced by a weak field-strength cation binding site that favors
334 permeation of easily dehydrated larger ions. Molecular dynamics (MD) simulations
335 show that the TRPV1 pore may contain up to four binding sites for monovalent cation
336 permeation in which the free energy for Na^+ and K^+ is very similar (Jorgensen et al.,
337 2016), consistent with the almost identical permeability ratio for Na^+ and K^+.
338 However, no definitive permeation mechanism has been dilucidated for TRPV
339 channels.

340 Our data suggest that while non-selective, the pore of TRPV1 channels can regulate
341 the flux of monovalent cations based on the energetics of dehydration and can
342 differentiate between the size of ions, which is borne by the permeability sequence
343 obtained from single-channel records (Figure 2A).

344 While MD simulations have suggested a highly flexible selectivity filter in TRPV1
345 (Darré et al., 2015), our results indicated that filter dynamics can be modulated by the
346 permeant ion. These results prompted us to explore the kinetics of transitions near
347 the open state. To this end, we employ the extended beta distribution method to
348 extract rate constants that arise from incomplete closures since simpler detection
349 methods such as half-amplitude threshold crossing are not appropriate to detect rapid
350 incomplete closings.

351 In single-channel recording experiments, we observed that the rapid transitions near
352 the open channel seems to speed up when large ions permeate, leading to increased
353 open channel noise. This observation could be explained if small ions like Li^+ and Na^+
354 are able to remain bound for longer times to the selectivity filter, due to their stronger
355 electrostatic electric field, and thus stabilize the open state, reducing fluctuations. This
356 is also consistent with the observation that smaller ions promote a higher open
357 probability (Fig. 3).

358 The rapid fluctuations we observe are consistent with the existence of transitions
359 from the open state to closed states that are adjacent to the open state. It is likely that
360 these represent rapid pore dynamics derived from structural transitions. Cryo-EM
361 experiments have revealed that many TRPV channels, including TRPV1, can exist in
362 different pore conformations, even in the presence of activators (Zhang et al., 2021).
363 Functional data have also provided evidence that TRPV channels can adopt different
364 open conformations in the presence of different ligands (Benítez-Angeles et al., 2023;
365 Canul-Sánchez et al., 2018).

366 Experiments employing single-molecule FRET in Kir channels have directly shown
367 dynamic changes of the structure of the selectivity filter as a function of the presence
368 of Na^+ or K^+ ions (Wang et al., 2019). Similar experiments employing solution nuclear
369 magnetic resonance have shown similar ion-dependent dynamics of the filter of non-
370 selective ion channel, which have a filter structure more closely related to TRPV1's
371 (Lewis et al., 2021) and the intrinsic pore dynamics of TRPV1 has been demonstrated
372 directly by measuring the fluorescence of genetically encoded non-canonical amino
373 acids (Steinberg et al., 2017).

374 An open question in TRPV channel biophysics, specially TRPV1, is the origin of the
375 mild voltage dependence of the macroscopic conductance. As mentioned before, the
376 VLSD does not support a canonical function as a voltage sensor (Palovcak et al.,
377 2015b). It has recently been proposed that a conformational change that rearranges
378 the position of negatively charged residues at the extracellular entrance of the
379 selectivity filter is responsible for the voltage dependence of TRPV1 gating, which is

equivalent to the displacement of ~0.55 elementary charges per channel. We find that in the presence of saturating capsaicin, the apparent gating charge depends on the identity of the permeant ion. The smallest alkali metal, Li^+, is associated with a steeper G-V, with an apparent gating charge of 0.65 e_o as well as activation at more negative voltages.

It is known that other types of ion channels obtain their voltage-dependence from the concerted movements of permeant ions in the permeation pathway (Schewe et al., 2016; Marchesi et al., 2012; Pusch et al., 1995) and that permeant blockers, also moving in the pore's electric field, can produce highly voltage-dependent block (Spassova and Lu, 1998). For example, in chloride ClC channels, voltage dependence is a result of the interaction of Cl^- ions with a protopore gate (Richard and Miller, 1990) and in Kir channels where permeating ions non-canonically regulate the voltage-dependence of gating in these channels (Lu et al., 2001; Kurata et al., 2010).

A fascinating observation derived from our study is that at relatively low concentration of capsaicin, were the open probability P_o ~0.4, the apparent gating charge is largest for the larger permeant cations, while at saturating concentration, with P_o = 0.98, the apparent gating charge is largest when the smaller ion (Li^+) permeates.

Acknowledgments

We thank Gisela Rangel, Manuel Hernández and Elsa Evaristo for excellent technical support. This work was supported by DGAPA-PAPIIT-UNAM grant No. IN215621. M. G-A is a doctoral student from Programa de Doctorado en Ciencias Bioquímicas-UNAM and was supported by a doctoral thesis scholarship from CONACyT No. 776082.

References

406 Benítez-Angeles, M., A.E.L. Romero, I. Llorente, I. Hernández-Araiza, A. Vergara-Jaque, F.H. Real,
407 Ó.E. Gutiérrez Castañeda, M. Arciniega, L.E. Morales-Buenrostro, F. Torres-Quiroz, R.
408 García-Villegas, L.B. Tovar-Y-Romo, W.B. Liedtke, L.D. Islas, and T. Rosenbaum. 2023.
409 Modes of action of lysophospholipids as endogenous activators of the TRPV4 ion channel.
410 *J. Physiol.* 601:1655–1673. doi:10.1113/JP284262.

411 Canul-Sánchez, J.A., I. Hernández-Araiza, E. Hernández-García, I. Llorente, S.L. Morales-Lázaro, L.D.
412 Islas, and T. Rosenbaum. 2018. Different agonists induce distinct single-channel
413 conductance states in TRPV1 channels. *J. Gen. Physiol.* 150:1735–1746.
414 doi:10.1085/jgp.201812141.

415 Cao, E. 2020. Structural mechanisms of transient receptor potential ion channels. *J. Gen. Physiol.*
416 152:e201811998. doi:10.1085/jgp.201811998.

417 Caterina, M.J., and D. Julius. 2001. The Vanilloid Receptor: A Molecular Gateway to the Pain
418 Pathway. *Annu. Rev. Neurosci.* 24:487–517. doi:10.1146/annurev.neuro.24.1.487.

419 Caterina, M.J., M.A. Schumacher, M. Tominaga, T.A. Rosen, J.D. Levine, and D. Julius. 1997a. The
420 capsaicin receptor: a heat-activated ion channel in the pain pathway. *Nature*. 389:816–
421 824. doi:10.1038/39807.

422 Caterina, M.J., M.A. Schumacher, M. Tominaga, T.A. Rosen, J.D. Levine, and D. Julius. 1997b. The
423 capsaicin receptor: a heat-activated ion channel in the pain pathway. *Nature*. 389:816–
424 824. doi:10.1038/39807.

425 Colquhoun, D., and F.J. Sigworth. 1995a. Fitting and Statistical Analysis of Single-Channel Records.
426 *In* Single-Channel Recording. B. Sakmann and E. Neher, editors. Springer US, Boston, MA.
427 483–587.

428 Colquhoun, D., and F.J. Sigworth. 1995b. Fitting and Statistical Analysis of Single-Channel Records.
429 *In* Single-Channel Recording. B. Sakmann and E. Neher, editors. Springer US, Boston, MA.
430 483–587.

431 Darré, L., S. Furini, and C. Domene. 2015. Permeation and dynamics of an open-activated TRPV1
432 channel. *J. Mol. Biol.* 427:537–549.

433 Deng, Z., N. Paknejad, G. Maksaev, M. Sala-Rabanal, C.G. Nichols, R.K. Hite, and P. Yuan. 2018.
434 Cryo-EM and X-ray structures of TRPV4 reveal insight into ion permeation and gating
435 mechanisms. *Nat. Struct. Mol. Biol.* 25:252–260. doi:10.1038/s41594-018-0037-5.

436 Eisenman, G. 1962. Cation selective glass electrodes and their mode of operation. *Biophys. J.*
437 2:259–323. doi:10.1016/s0006-3495(62)86959-8.

438 Fitzhugh, R. 1983. Statistical properties of the asymmetric random telegraph signal, with
439 applications to single-channel analysis. *Math. Biosci.* 64:75–89. doi:10.1016/0025-
440 5564(83)90028-7.

441 Geron, M., R. Kumar, W. Zhou, J.D. Faraldo-Gómez, V. Vásquez, and A. Priel. 2018. TRPV1 pore
442 turret dictates distinct DkTx and capsaicin gating. *Proc. Natl. Acad. Sci.* 115.
443 doi:10.1073/pnas.1809662115.

444 Grandl, J., S.E. Kim, V. Uzzell, B. Bursulaya, M. Petrus, M. Bandell, and A. Patapoutian. 2010.
445 Temperature-induced opening of TRPV1 ion channel is stabilized by the pore domain. *Nat.*
446 *Neurosci.* 13:708–714.

447 Hamill, O.P., A. Marty, E. Neher, B. Sakmann, and F.J. Sigworth. 1981. Improved patch-clamp
448 techniques for high-resolution current recording from cells and cell-free membrane
449 patches. *Pflugers Arch*. 391:85–100.

450 Heinemann, S.H., and F.J. Sigworth. 1991. Open channel noise. VI. Analysis of amplitude
451 histograms to determine rapid kinetic parameters. *Biophys. J.* 60:577–587.
452 doi:10.1016/S0006-3495(91)82087-2.

453 Hui, K., B. Liu, and F. Qin. 2003. Capsaicin activation of the pain receptor, VR1: multiple open
454 states from both partial and full binding. *Biophys. J.* 84:2957–2968. doi:10.1016/S0006-
455 3495(03)70022-8.

456 Jara-Oseguera, A., C. Bae, and K.J. Swartz. 2016. An external sodium ion binding site controls
457 allosteric gating in TRPV1 channels. *eLife*. 5:e13356. doi:10.7554/eLife.13356.

458 Jara-Oseguera, A., K.E. Huffer, and K.J. Swartz. 2019. The ion selectivity filter is not an activation
459 gate in TRPV1-3 channels. *Elife*. 8:e51212.

460 Jara-Oseguera, A., and K.J. Swartz. 2015. Unraveling Allosteric Coupling Mechanisms in the TRPV1
461 Channel. *Biophys. J.* 108:124a. doi:10.1016/j.bpj.2014.11.695.

462 Jordt, S.-E., M. Tominaga, and D. Julius. 2000. Acid potentiation of the capsaicin receptor
463 determined by a key extracellular site. *Proc. Natl. Acad. Sci.* 97:8134–8139.
464 doi:10.1073/pnas.100129497.

465 Jorgensen, C., S. Furini, and C. Domene. 2016. Energetics of Ion Permeation in an Open-Activated
466 TRPV1 Channel. *Biophys. J.* 111:1214–1222. doi:10.1016/j.bpj.2016.08.009.

467 Kurata, H.T., M. Rapedius, M.J. Kleinman, T. Baukrowitz, and C.G. Nichols. 2010. Voltage-
468 dependent gating in a "voltage sensor-less" ion channel. *PLoS Biol.* 8:e1000315.
469 doi:10.1371/journal.pbio.1000315.

470 Lewis, A., V. Kurauskas, M. Tonelli, and K. Henzler-Wildman. 2021. Ion-dependent structure,
471 dynamics, and allosteric coupling in a non-selective cation channel. *Nat. Commun.*
472 12:6225. doi:10.1038/s41467-021-26538-8.

473 Liao, M., E. Cao, D. Julius, and Y. Cheng. 2013. Structure of the TRPV1 ion channel determined by
474 electron cryo-microscopy. *Nature*. 504:107–112. doi:10.1038/nature12822.

475 Lu, T., L. Wu, J. Xiao, and J. Yang. 2001. Permeant ion-dependent changes in gating of Kir2.1
476 inward rectifier potassium channels. *J. Gen. Physiol.* 118:509–522.
477 doi:10.1085/jgp.118.5.509.

478 Marchesi, A., M. Mazzolini, and V. Torre. 2012. Gating of cyclic nucleotide-gated channels is
479 voltage dependent. *Nat. Commun.* 3:973. doi:10.1038/ncomms1972.

480 Matta, J.A., and G.P. Ahern. 2007. Voltage is a partial activator of rat thermosensitive TRP
481 channels: Voltage-independent gating of TRPV1 and TRPM8. *J. Physiol.* 585:469–482.
482 doi:10.1113/jphysiol.2007.144287.

483 Numazaki, M., T. Tominaga, K. Takeuchi, N. Murayama, H. Toyooka, and M. Tominaga. 2003.
484 Structural determinant of TRPV1 desensitization interacts with calmodulin. *Proc. Natl.*
485 *Acad. Sci. U. S. A.* 100:8002–8006. doi:10.1073/pnas.1337252100.

486 Palovcak, E., L. Delemotte, M.L. Klein, and V. Carnevale. 2015a. Comparative sequence analysis
487 suggests a conserved gating mechanism for TRP channels. *J. Gen. Physiol.* 146:37–50.

488 Palovcak, E., L. Delemotte, M.L. Klein, and V. Carnevale. 2015b. Comparative sequence analysis
489 suggests a conserved gating mechanism for TRP channels. *J. Gen. Physiol.* 146:37–50.

490 Pusch, M., U. Ludewig, A. Rehfeldt, and T.J. Jentsch. 1995. Gating of the voltage-dependent
491 chloride channel CIC-0 by the permeant anion. *Nature*. 373:527–531.
492 doi:10.1038/373527a0.

493 Rauh, O., U.-P. Hansen, S. Mach, A.J.W. Hartel, K.L. Shepard, G. Thiel, and I. Schroeder. 2017.
494 Extended beta distributions open the access to fast gating in bilayer experiments-assigning
495 the voltage-dependent gating to the selectivity filter. *FEBS Lett.* 591:3850–3860.
496 doi:10.1002/1873-3468.12898.

497 Rauh, O., U.P. Hansen, D.D. Scheub, G. Thiel, and I. Schroeder. 2018. Site-specific ion occupation in
498 the selectivity filter causes voltage-dependent gating in a viral K+ channel. *Sci. Rep.*
499 8:10406. doi:10.1038/s41598-018-28751-w.

500 Richard, E.A., and C. Miller. 1990. Steady-state coupling of ion-channel conformations to a
501 transmembrane ion gradient. *Science*. 247:1208–1210. doi:10.1126/science.2156338.

502 Rosenbaum, T., A. Gordon-Shaag, M. Munari, and S.E. Gordon. 2004. Ca2+/Calmodulin Modulates
503 TRPV1 Activation by Capsaicin. *J. Gen. Physiol.* 123:53–62. doi:10.1085/jgp.200308906.

504 Rosenbaum, T., S.L. Morales-Lázaro, and L.D. Islas. 2022. TRP channels: a journey towards a
505 molecular understanding of pain. *Nat. Rev. Neurosci.* 23:596–610. doi:10.1038/s41583-
506 022-00611-7.

507 Salazar, H., A. Jara-Oseguera, E. Hernandez-Garcia, I. Llorente, I.I. Arias-Olguin, M. Soriano-Garcia,
508 L.D. Islas, and T. Rosenbaum. 2009. Structural determinants of gating in the TRPV1
509 channel. *Nat. Struct. Mol. Biol.* 16:704–710.

510 Samways, D.S.K., and T.M. Egan. 2011. Calcium-dependent decrease in the single-channel
511 conductance of TRPV1. *Pflüg. Arch. - Eur. J. Physiol.* 462:681–691. doi:10.1007/s00424-
512 011-1013-7.

513 Schewe, M., E. Nematian-Ardestani, H. Sun, M. Musinszki, S. Cordeiro, G. Bucci, B.L. de Groot, S.J.
514 Tucker, M. Rapedius, and T. Baukrowitz. 2016. A Non-canonical Voltage-Sensing
515 Mechanism Controls Gating in K2P K+ Channels. *Cell*. 164:937–949.
516 doi:10.1016/j.cell.2016.02.002.

517 Schroeder, I. 2015. How to resolve microsecond current fluctuations in single ion channels: The
518 power of beta distributions. *Channels*. 9:262–280. doi:10.1080/19336950.2015.1083660.

519 Shimada, H., T. Kusakizako, T.H. Dung Nguyen, T. Nishizawa, T. Hino, M. Tominaga, and O. Nureki.
520 2020. The structure of lipid nanodisc-reconstituted TRPV3 reveals the gating mechanism.
521 *Nat. Struct. Mol. Biol.* 27:645–652. doi:10.1038/s41594-020-0439-z.

522 Spassova, M., and Z. Lu. 1998. Coupled Ion Movement Underlies Rectification in an Inward-
523 Rectifier K+ Channel. *J. Gen. Physiol.* 112:211–221. doi:10.1085/jgp.112.2.211.

524 Steinberg, X., M.A. Kasimova, D. Cabezas-Bratesco, J.D. Galpin, E. Ladron-de-Guevara, F. Villa, V.
525 Carnevale, L. Islas, C.A. Ahern, and S.E. Brauchi. 2017. Conformational dynamics in TRPV1
526 channels reported by an encoded coumarin amino acid. *eLife*. 6:e28626.
527 doi:10.7554/eLife.28626.

528 Wang, S., S.-J. Lee, G. Maksaev, X. Fang, C. Zuo, and C.G. Nichols. 2019. Potassium channel
529 selectivity filter dynamics revealed by single-molecule FRET. *Nat. Chem. Biol.* 15:377–383.
530 doi:10.1038/s41589-019-0240-7.

531 Yang, F., L. Xu, B.H. Lee, X. Xiao, V. Yarov-Yarovoy, and J. Zheng. 2020. An Unorthodox Mechanism
532 Underlying Voltage Sensitivity of TRPV1 Ion Channel. *Adv. Sci.* 7:2000575.
533 doi:10.1002/advs.202000575.

534 Yellen, G. 1984. Ionic permeation and blockade in Ca2+-activated K+ channels of bovine
535 chromaffin cells. *J. Gen. Physiol.* 84:157–186. doi:10.1085/jgp.84.2.157.

536 Yu, F.H., and W.A. Catterall. 2004. The VGL-Chanome: A Protein Superfamily Specialized for
537 Electrical Signaling and Ionic Homeostasis. *Sci. STKE*. 2004. doi:10.1126/stke.2532004re15.

538 Zhang, K., D. Julius, and Y. Cheng. 2021. Structural snapshots of TRPV1 reveal mechanism of
539 polymodal functionality. *Cell.* 184:5138-5150.e12. doi:10.1016/j.cell.2021.08.012.

540 Zubcevic, L., S. Le, H. Yang, and S.-Y. Lee. 2018. Conformational plasticity in the selectivity filter of
541 the TRPV2 ion channel. *Nat. Struct. Mol. Biol.* 25:405–415. doi:10.1038/s41594-018-0059-
542 z.

543

544

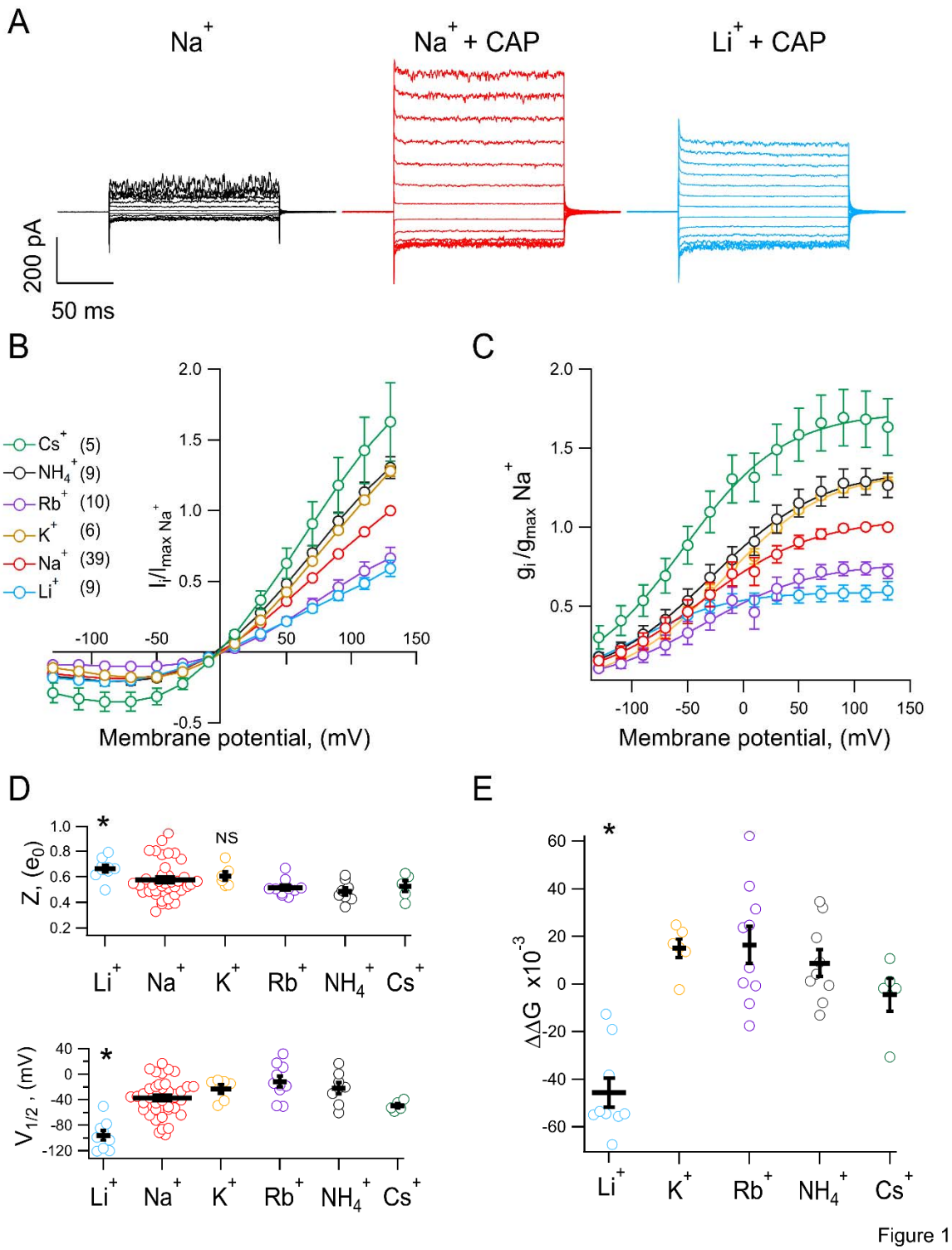

Figure 1. The voltage dependence of TRPV1 is influenced by the permeant ion.

A) Representative inside-out current-traces recorded in the same patch, elicited by 20 mV steps from -130 mV to 130 mV for a duration of 150 ms. The extracellular solution (pipette) contained 130 mM NaCl, this patch was first exposed to internal 130 mM

NaCl (black) followed by exposure to 130 mM NaCl + 10 μM capsaicin (red) and finally to 130 mM LiCl + 10 μM capsaicin (blue). All experiments were performed following the same experimental strategy to compare the permeation of different monovalent ions (Li^+, K^+, Rb^+, NH_4^+, Cs^+) with respect to the permeation of Na^+ in the same patch. **B)** Averages of current-voltage (I-V) relations for all ions tested. The number of experiments, n, is in parenthesis. **C)** Conductance-voltage (G-V) relations for monovalent ions, obtained from data as in B in the presence of 10 μM capsaicin, normalized to data with a symmetrical concentration of Na^+ from each patch. G-V relations were fitted to the Boltzmann function (lines). **D)** Scatter plots of the apparent charge (Z; above) and $V_{½}$ (below) associated with channel opening, both were estimated by fitting a Boltzmann function to G-V curves in B. The values of Z for Li^+ were compared for statistical differences with all other ions, the p values are: *p = 0.00007 for Li^+ vs. Na^+; NS (not significant) p=0.213 for Li^+ vs. K^+; *p = 0.00034 for Li^+ vs. Rb^+; *p = 0.00005 for Li^+ vs. NH_4^+; *P = 0.01 for Li^+ vs. Cs^+. For $V_{½}$: *p = 0.0000009 for Li^+ vs. Na^+; *p = 0.00001 for Li^+ vs. K^+; *p = 0.00000001 for Li^+ vs. Rb^+; *P = 0.000002 for Li^+ vs. NH_4^+; *p = 0.02 for Li^+ vs. Cs^+. **E)** Scatter plot of the $\Delta\Delta G$ associated to the ion effect in channel opening was estimated as: $\Delta\Delta G = \Delta G_{Ion} - \Delta G_{Na^+}$ the data was taken from the fit in B. *p = 0.00005 for Li^+ vs. K^+; *p = 0.0000002 for Li^+ vs. Rb^+; *p = 0.000004 for Li^+ vs. NH_4^+; *p = 0.003 for Li^+ vs. Cs^+. Data are shown as mean ± SEM. The significant difference was determined with a one-way ANOVA test followed by a Tukey´s test post-hoc (*p < 0.05).

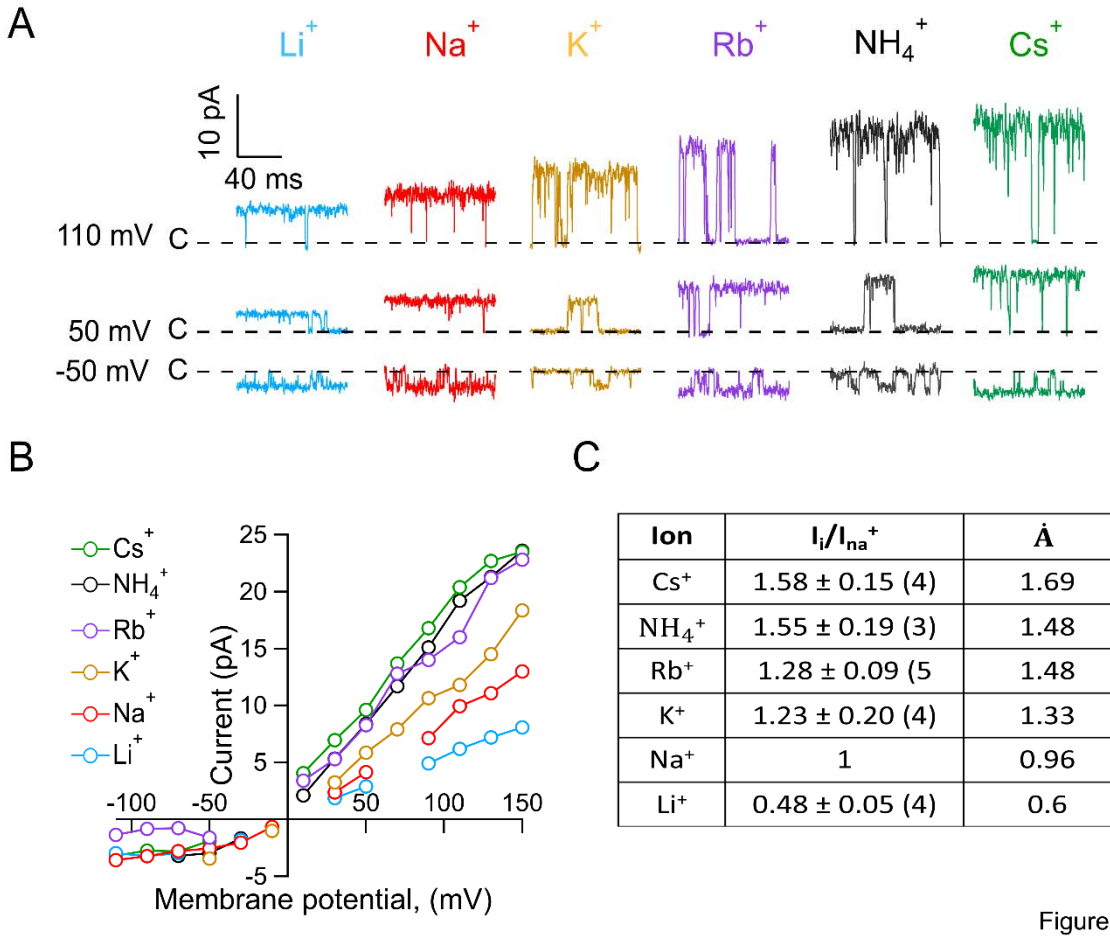

Ion	I_i/I_{na}^+	Å
Cs^+	1.58 ± 0.15 (4)	1.69
NH_4^+	1.55 ± 0.19 (3)	1.48
Rb^+	1.28 ± 0.09 (5	1.48
K^+	1.23 ± 0.20 (4)	1.33
Na^+	1	0.96
Li^+	0.48 ± 0.05 (4)	0.6

Figure 2

Figure 2. TRPV1 permeability to monovalent ions is size-dependent.

A) Representative current traces showing openings from longer single-channel recordings in the presence of varying permeant ions. Inside-out patches were first exposed to internal 130 mM Na^+ + 100 nM capsaicin and then to internal 130 mM (Li^+ (blue), Na^+ (red) K^+(mustard), Rb^+ (purple), NH_4^+ (black), Cs^+ (green)) + 100 nM capsaicin similarly to experiments in Figure 1A. The dashed line represents the closed state of the channel. B) Representative I-V relations from single-channel records. These were obtained from data as in A for each ion. C) Current carried by each ion relative to the single-channel current amplitude with Na^+. Ionic radii in Å are also shown for comparison. Data are mean ± SEM, n is shown in parentheses.

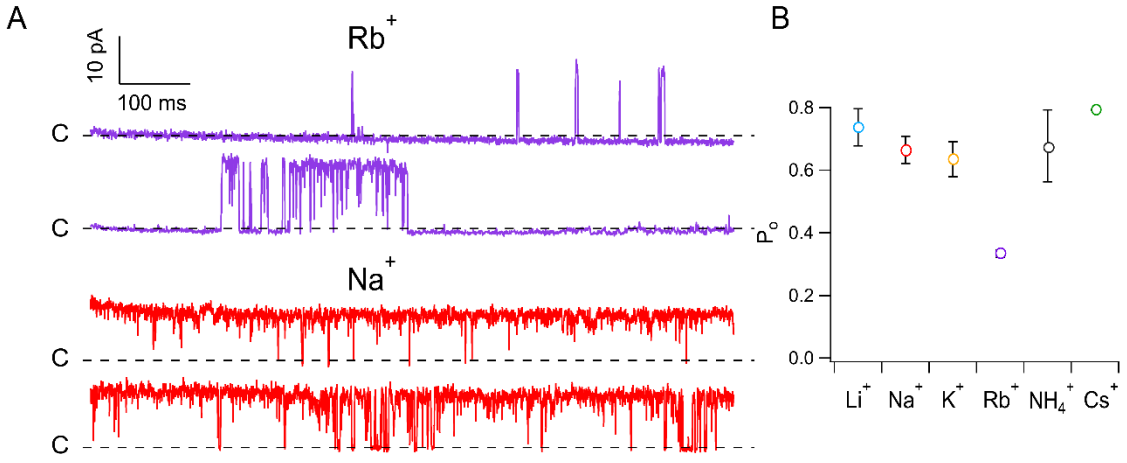

Figure 3

Figure 3. Rubidium ions strongly modulate the single-channel open probability of TRPV1 channels.

A) Representative current traces from single-channel recordings at 90 mV when intracellular Rb^+ (purple) or Na^+ (red) were used as permeant ions. B) Open probability of TRPV1 channels at 90 mV in the presence of different permeant ions and 100 nM of capsaicin, calculated from traces of current recordings as shown in A. Data are mean ± s.e.m.

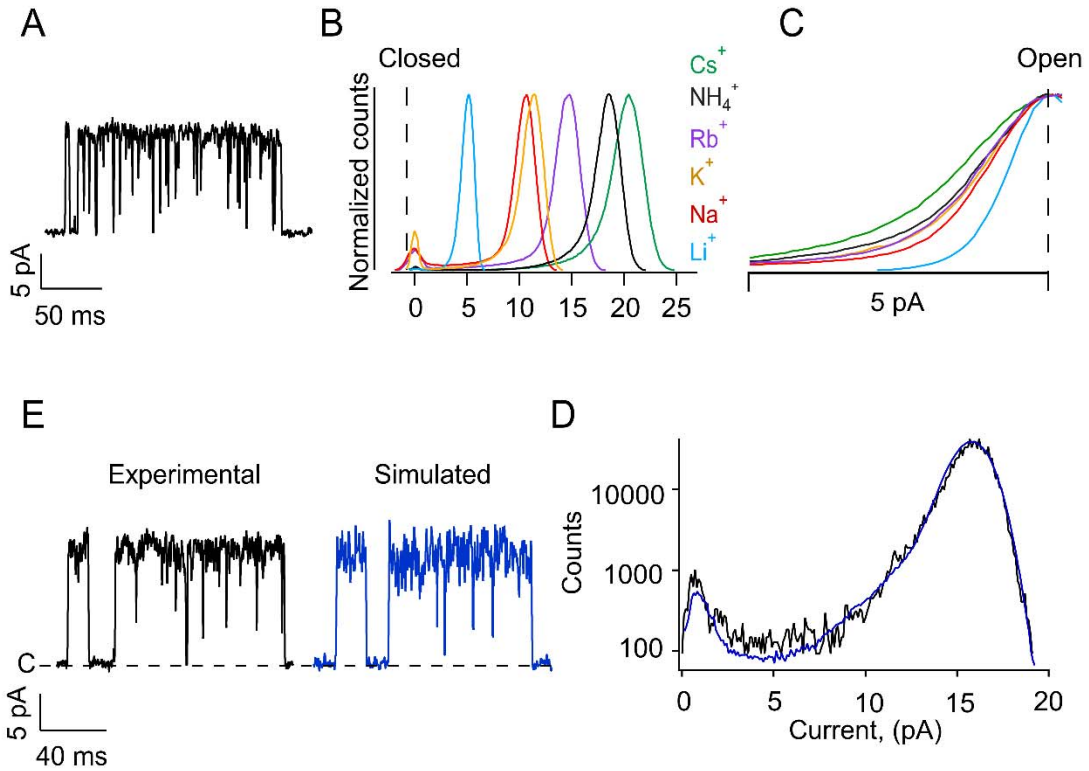

Figure 4

Figure 4. Fluctuations in the single-channel current during the open state can be fitted by a Markov model.

A) Representative current trace during a typical single TRPV1 opening burst recorded in the inside-out configuration at 90 mV, with internal 130 mM RbCl + 100 nM capsaicin. B) Normalized all-points histograms showing single-channel current amplitudes of openings elicited by 100 nM capsaicin at 90 mV, for each ion tested. The histograms are shown aligned to the closed state amplitude peak (left). C) Close-up of the tails of events of the all-points histograms in B aligned to the maximum current amplitude of the open state to highlight the asymmetric form of the histograms. D) Current trace of a single-channel at 90 mV from an inside-out patch exposed to internal 130 mM NH_4Cl + 100 nM capsaicin (black) and simulation with the model in Scheme I (blue). These simulated recordings are used to produce simulated all-points amplitude histograms of single-channel current, which are then fitted to experimental all-points amplitude histograms. E) Typical fit of a simulated histogram (blue) to experimental histogram from single current elicited by 110 mV with internal 130 mM NH_4Cl + 100 nM capsaicin (black) using the Markov model in Scheme I. Parameters obtained from the fit are: α_o = 1500; α_c = 27; β_o = 22500; β_c = 600; γ_o = 127500; γ_c = 30000; χ^2 = 0.00013873.

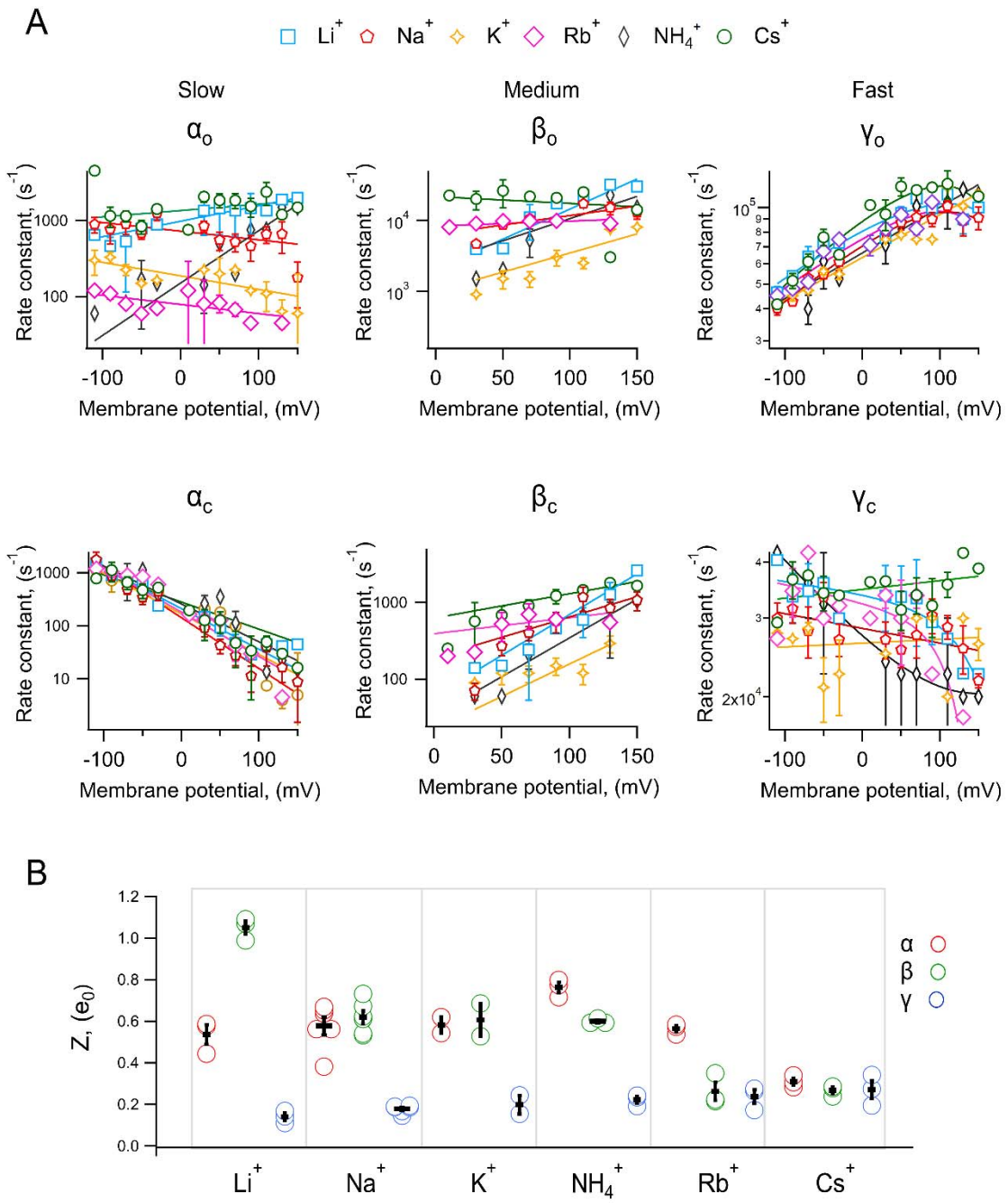

Figure 5

Figure 5. Voltage-dependent transitions near the open state of TRPV1 channels are modulated by the permeant ions.

A) Rate constants obtained from the Markov model fit to the histograms as in Figure 4D. The rate constants were classified as slow, medium, and fast according to their magnitude at 0 mV. The continuous curves represent the fit to Eq. 5 or 6.

B) Scatter plot of the sum of the apparent charge by transition (Z^i_c+Z^i_o where I = α, β or γ) obtained from the fit of equations 5 or 6 to rate constants in A. Black bars are mean ± s.e.m.

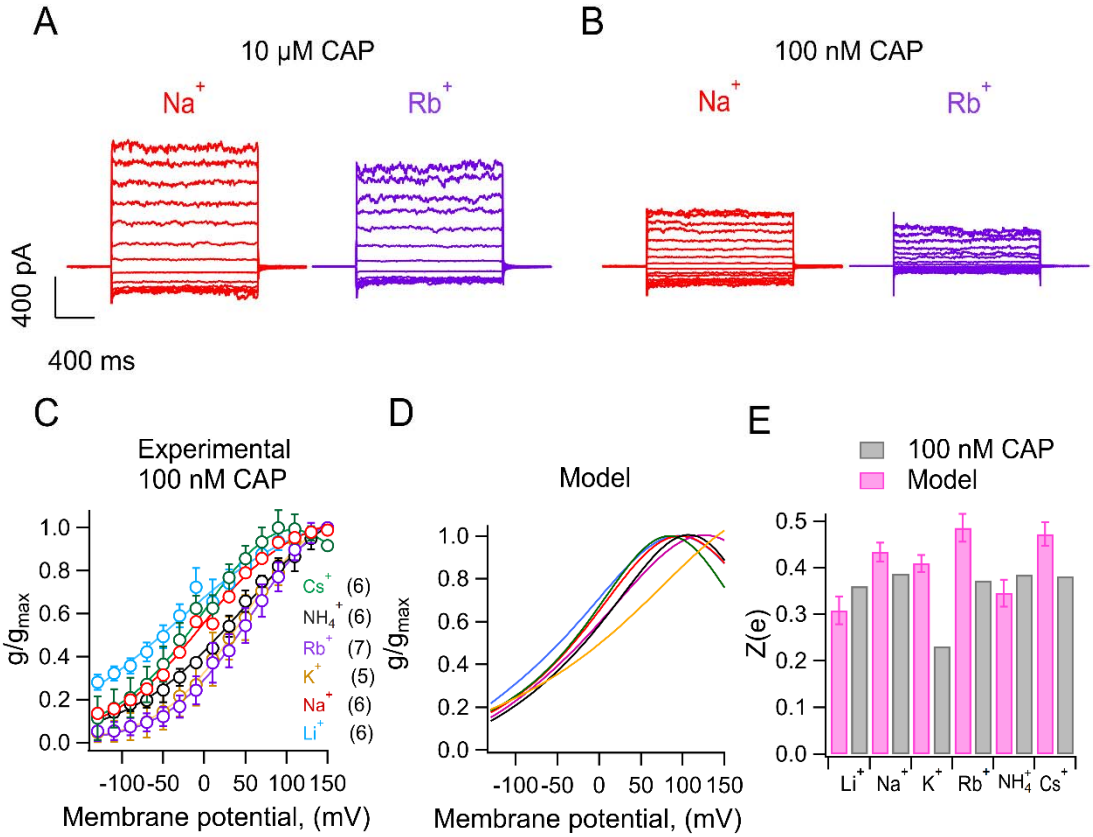

Figure 6

Figure 6. The opening probability predicted by the Markov model explains the macroscopic experimental behavior.

A) Representative inside-out macroscopic current traces recorded in the same patch, elicited by 20 mV steps from -130 mV for 150 ms. The patch was exposed to internal 130 mM NaCl + 10 μM capsaicin (red) followed by 130 mM RbCl + 10 μM capsaicin (purple). B) Representative inside-out current traces like A but using 100 nM capsaicin. C) Normalized conductance-voltage (G-V) relations with monovalent ions, obtained from inside-out patches after treatment with internal 100 nM capsaicin. The G-V relation was fitted to the Boltzmann function (line). Data are shown as mean ± s.e.m., number of experiments n, in parenthesis. D) Normalized prediction of open probability by a Markov model for each monovalent ion. E) Bar graph of apparent charge associated with channel opening estimated by fitting a Boltzmann equation to curves in A and B. Data is shown as mean ± s.e.m.

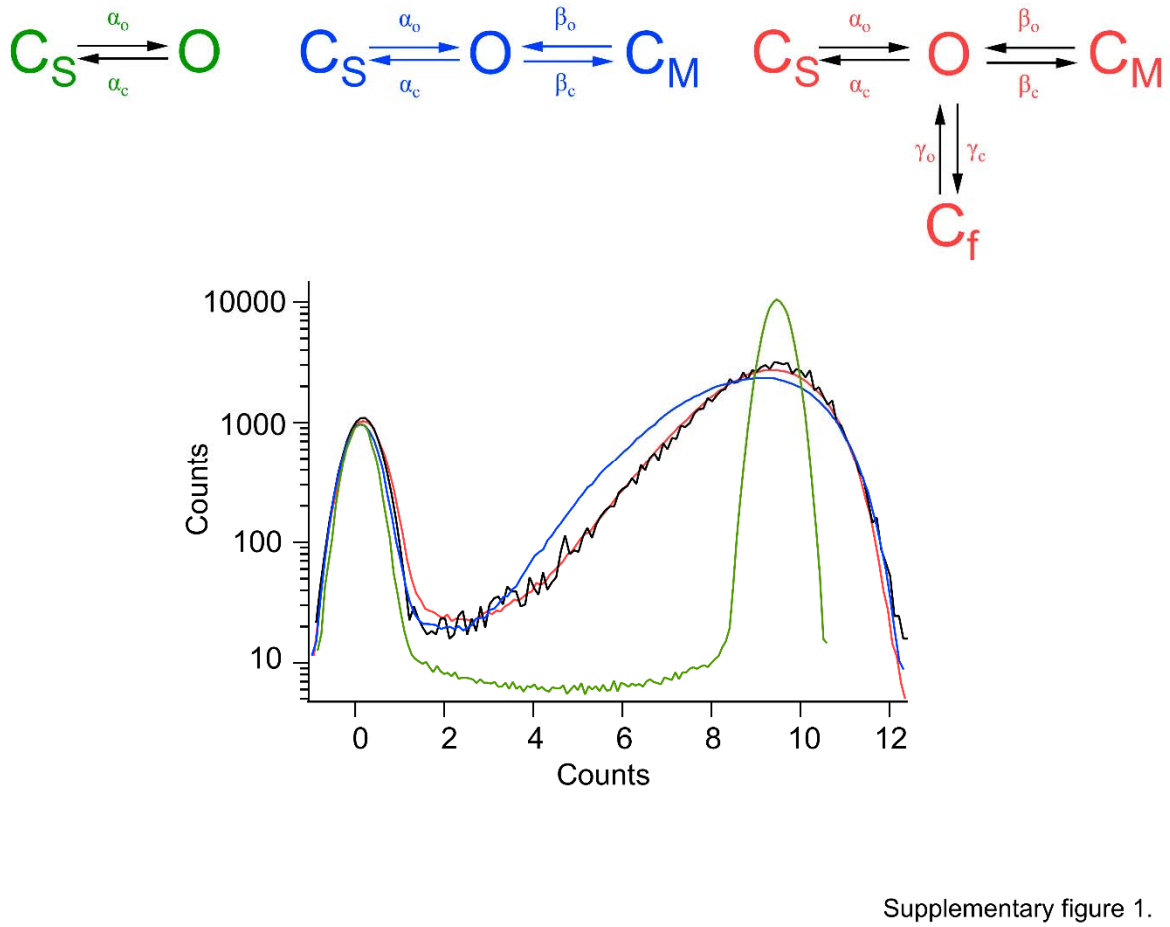

Supplementary Figure 1. Amplitude histogram fits to three different Markov models.

A) Markov models with 1 closed state (green), two closed states (blue) and three closed states (red). B) Fit of the simulated histograms from the models in A to experimental an all-points histogram of single channel current of TRPV1(black), elicited by a pulse to 90 mV from an inside-out patches exposed to 130 mM NaCl + 100 nM capsaicin. The fits parameters used for 1 close state were: α_o = 301.9535; α_c = 36.1664; χ^2 = 0.0697; 2 closed states α_o = 300; α_c = 37.5; γ_o = 28500; γ_c = 13500; χ^2 = 0.002342; three closed states α_o = 280.61; α_c = 49; β_o = 14724.475; β_c = 1133.16; γ_o = 52500; γ_c = 15396; χ^2 = 0.00017296.